Proceedings of the ASME 2019 Gas Turbine India
GTINDIA2019
December 5-6, 2019, Chennai, Tamil Nadu, India

GTINDIA2019-2604

DYNAMIC CHARACTERISTICS OF A FLEXIBLE COUPLING

Mohit Aggarwal[1], J.K. Dutt
Department of Mechanical Engineering, IIT Delhi
New Delhi 110016, India

S. Chandraker
Department of Mechanical Engineering, NIT
Surathkal, Mangalore 575025, India

ABSTRACT

Flexible couplings are used to transmit power between two shafts and accommodate, more realistically, a combination of parallel, axial and angular misalignments, between them. Presence of misalignment of certain degree is considered unavoidable. The coupling also attenuates the transmission of fluctuation of torque and speed from one rotor to the other by flexing itself, and is thus helpful in providing nearly smooth transmission of speed and torque. However, in this process, the dynamic behavior of the rotors is also influenced by the coupling characteristics, as the coupling incorporates a flexible damped intermediate member between the shafts it couples. A detailed literature survey has shown that researchers so far have not attempted to find out the dynamic characteristics, the stiffness and damping of a coupling, and, instead, the effect of misalignment (combination of parallel and angular misalignment) is considered to generate forces independent of the coupling characteristics. This paper attempts to find out an analytical model for the dynamic characteristic of segmented link coupling in terms of suitable non-dimensional coefficients to generate the characteristics of a coupling element which may be used for dynamic analysis of coupled rotor shaft system.

Keywords: flexible coupling, stiffness and damping of flexible coupling, model of segmented link coupling.

INTRODUCTION

Misalignment occurs when the driving and the driven shafts of any rotating machinery are not in the same centerline. A combination of parallel, angular and axial misalignment is thus taken care by the flexible couplings. Flexible element itself flexes to accommodate misalignment has its own characteristics, stiffness and damping, present in the spin synchronized frame of the rotor, and thus, influence the system to which it is connected. This work, in the first place attempts to find the coupling characteristics, by considering generic viscoelastic constitutive behavior of the links, which, in many cases are made of polymeric composites, to make the coupling light, yet useful. The properties of the segmented discs is first determined by testing the material using a Dynamic Mechanical Analyzer (DMA) and then the multi-element viscoelastic model of the material is extracted. This allows to represent the viscoelastic modulus as an operator. Next, the principle of beam theory is used to derive the stiffness operator for one segmented disc under different deformations (parallel, angular and axial) and then, these stiffness operators are assembled properly to determine theoretically the stiffness and dissipation behavior of the coupling. It may be pointed out that the information of dissipation behavior of the coupling is expressed by the differential stiffness operator. However, within the literature surveyed so far, there was hardly any reported attempt to present the dynamic characteristics, stiffness and dissipation behavior, of a disc coupling. This gap inspired this activity.

Gibbons [1] proposed a formulation of misalignment forces of the coupling. Later, many researchers adopted force equations based on the analysis proposed by the author. Sekhar and Prabhu [2] evaluated the effect of coupling misalignment on vibration response of a rotor, by including the forces imposed by the coupling, based on the formulation given by Gibbons [1]. In doing so, the authors took care of only the static value of the misalignment to model the forces, and also, no attempt was made to obtain the stiffness and damping of the coupling, thus they could not study the effect of coupling characteristics on the stability and response of the rotor shaft system as the coupling characteristics did not enter into the system matrix and the modal characteristic of the system were not influenced. Xu and Marangoni [3] derived misalignment forces based on kinematics

[1] Contact author: romit589@gmail.com

of the Hooke's joint, and concluded that shaft-misalignment produces even multiple of the spin frequency of the rotor. However, again, the authors did not find the coupling characteristics (stiffness and damping) and include them in the equations of motion of the rotor shaft system. Patel and Darpe [4] proposed a stiffness model by using experimentally measured data on forces induced due to both parallel and angular misalignment. The authors provided only the stiffness matrix of the coupling and the damping matrix was assumed to be proportional in nature. No attempt was reported to obtain the damping matrix of the coupling. Although, the authors provided stiffness matrix, there was no mathematical model to derive stiffness, thus making the exercise coupling specific and experiment dependent.

All these reasons inspired the authors to work on building a mathematical model to derive the stiffness and damping matrices for a coupling, and in particular, the segmented disc type coupling, which is very widely used in industries. A good contribution of this work is that, suitable non-dimensional parameters have been identified to present the stiffness operators to make such models useful irrespective of the shape and size of the coupling. So this paper reports these non-dimensional stiffness operators of a segmented disc type coupling, and shows numerical examples of the variation of its stiffness and damping, for different number of segments, link dimension and link material. The stiffness matrix, in the differential operator form may be used to represent a coupling in a rotor-shaft system to model the dynamic behavior of rotor in a spin-synchronized reference frame.

1 Analysis

The analysis in the section below, is carried out under two sub-sections. Firstly, the viscoelastic model for the coupling material is extracted with the help of DMA and the values of variables for different parametric models are obtained by curve fitting and optimization. Secondly, the lateral and bending stiffness for the segmented disc coupling is derived from parallel and angular misalignment respectively.

1.1 Model Extraction

Viscoelasticity is a property, wherein, a material exhibits the characteristic of both fluid and solid and this combined material behavior is represented by a combination of springs and dampers, and thus, the corresponding constitutive relation is obtained. Dynamical Mechanical Analyzer, or DMA, is a machine that mechanically deforms a material sample and measures its response, as a function of temperature, time or frequency. A multi frequency test on single cantilever setup was performed on TA instruments QDMA 800 machine to obtain the variation of storage and loss moduli with the frequency of excitation. Various models were then fitted on the data and seven parameter Wiechert model was found to be most suitable within the specified error limits.

The storage and dissipation energy due to dynamic deformation of viscoelastic material is frequency dependent, and is obtained by following an operator based approach, as proposed by Dutt and Roy [5], where stiffness is represented in the form of differential operator of time.

$$E^*(\ ) = E_\infty + \sum_{j=1}^{j=n} \frac{E_j\, D}{\left(\frac{E_j}{\eta_j} + D\right)} \tag{1}$$

Following Brinson [6], the frequency dependent complex modulus (E*) for the Weichert model is obtained as

$$E^*(w) = E_s(w) + i\, E_l(w) \tag{2}$$

$$E_s \text{ (storage modulus)} = E_\infty + \sum_{j=1}^{j=n} \frac{E_j\, w^2}{\left(\frac{E_j}{\eta_j}\right)^2 + w^2} \tag{3}$$

$$E_l \text{ (loss modulus)} = \sum_{j=1}^{j=n} \frac{E_j{}^2 \left(\frac{w}{\eta_j}\right)}{\left(\frac{E_j}{\eta_j}\right)^2 + w^2} \tag{4}$$

$$\tan(\varsigma) = E_l / E_s \tag{5}$$

The material has principal axis inclined along and perpendicular to the fiber as shown in the Fig. 1b), thus, DMA test is performed at Ψ = 0, 45 and 90 degree, here 1 and 2 denote the directions along and perpendicular to the fiber, Ψ denotes the angle made by fiber axes (1 and 2) with x axis. To extract the parameters E_∞, E_j and η_j (j = 1 to 3, in this case) for various models and non-linear optimization technique based on the principle of Generalized Reduced Gradient (GRG) method is used. The flow chart, Fig. 2, explains the method of finding the parameters.

Let E_{se}, E_{le}, $\tan(\varsigma)_e$ and E_{sm}, E_{sm}, $\tan(\varsigma)_m$ be the values obtained by experiment and model fitting respectively.

Objective function:

$$Z = \text{Min}\ (\sum(\tan(\varsigma)_e - \tan(\varsigma)_m)^2) \tag{6}$$

Constraints:

$$\text{Max. of Abs}(100*(E_{se} - E_{sm})/ E_{se}) \leq a \tag{7}$$
$$\text{Max. of Abs}(100*(E_{le} - E_{lm})/ E_{le}) \leq b$$

Variables: E_∞, E_j and η_j (j = 1 to 3) > 0 (8)

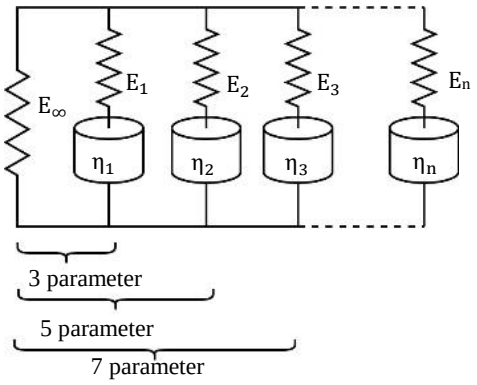

Fig. 1a): Wiechert Model

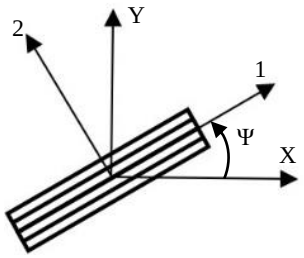

Fig. 1b): Fiber axes (1 and 2) w.r.t material axes (X and Y)

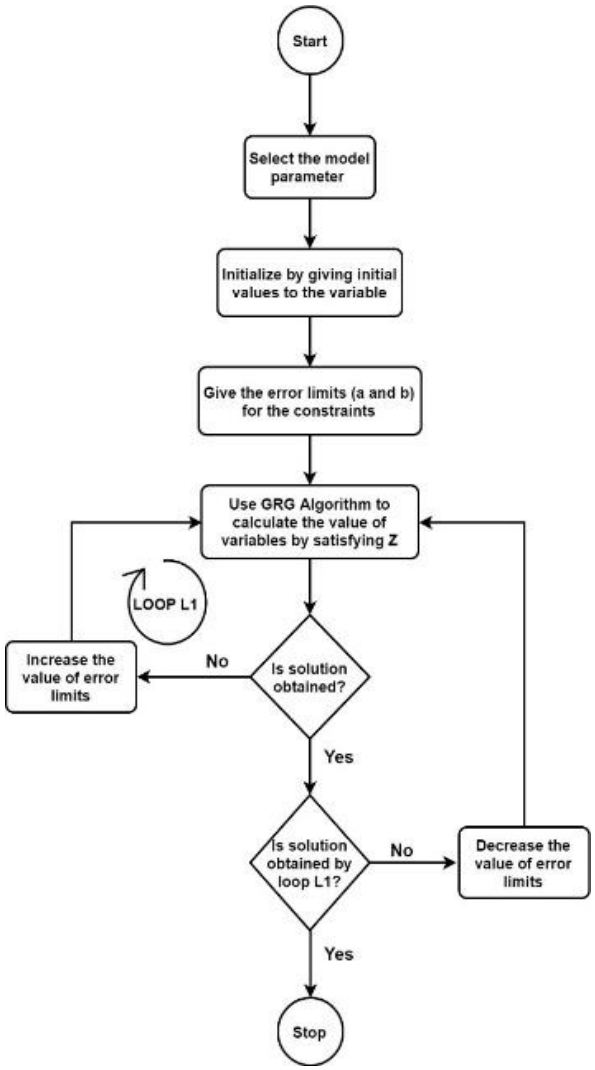

Fig. 2: Flow chart explaining the model extraction procedure

Tables [1-3] show extracted model in terms of the parameters E_∞, E_j and η_j (j = 1 to 3).The material of the coupling link used for the analysis was G11 FRP.

Table 1: Value of parameters for different models with fiber angle 0^0

Model Parameter	E_∞	E_1	E_2	E_3	η_1	η_2	η_3
3	14528.58	376.7628	-	-	1.5747	-	-
5	14399.33	263.2593	409.9384	-	22.6409	0.98109	-
7	14422.44	253.7447	104.4472	2.11 x 10^8	29.1921	1.2104	0.59086

Table 2: Value of parameters for different models with fiber angle 45^0

Model Parameter	E_∞	E_1	E_2	E_3	η_1	η_2	η_3
3	12518.09	332.9675	-	-	1.5091	-	-
5	12366.06	247.2794	354.9503	-	21.2314	0.8867	-
7	12356.26	229.6856	106.7878	4313882	28.98785	1.34913	0.52151

Table 3: Value of parameters for different models with fiber angle 90^0

Model Parameter	E_∞	E_1	E_2	E_3	η_1	η_2	η_3
3	12220.53	302.2567	-	-	1.19925	-	-
5	12082.3	216.844	348.385	-	18.5320	0.73099	-
7	12124.89	211.721	72.7008	2.24 x10^{15}	25.0762	0.79482	0.487737

Fig.[3-5] show the experimental data with the model fit data for 3, 5 and 7 parameter model with angle Ψ = 0, 45 and 90 degree. It is seen that as the no. of relaxation fields are increased the model is more accurately able to predict the behavior of the material. The maximum percentage error, table 4, shows that 7 parameter model most appropriately represents the material characteristic with error less than 10%.

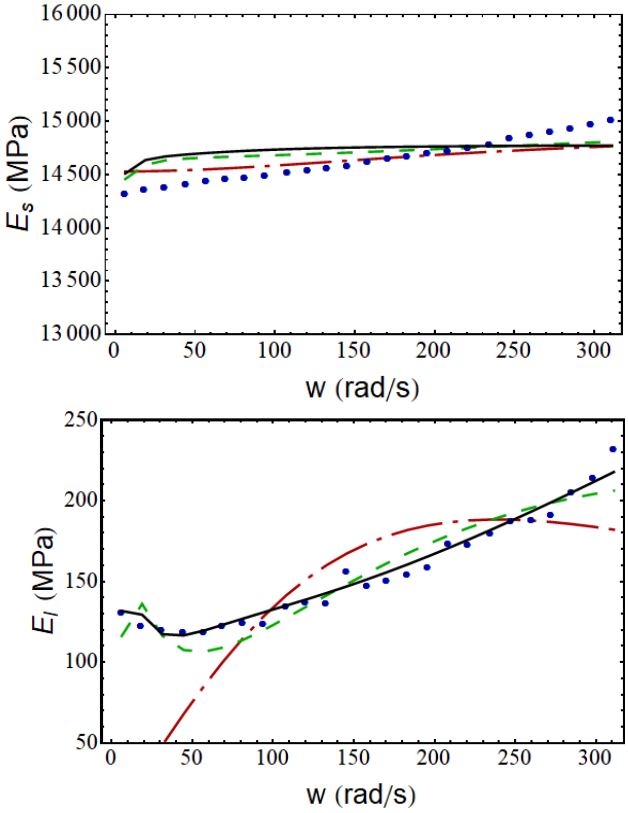

Fig. 3: Variation of storage (E_s) and loss moduli (E_l) with excitation frequency (w) for fiber angle (Ψ) = 0 degree.
Key: ..... Experimental data; – · – · – 3 parameter model; – – – – 5 parameter model; —— 7 parameter model.

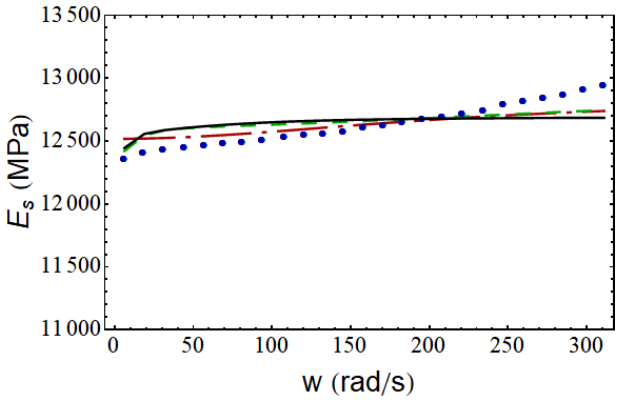

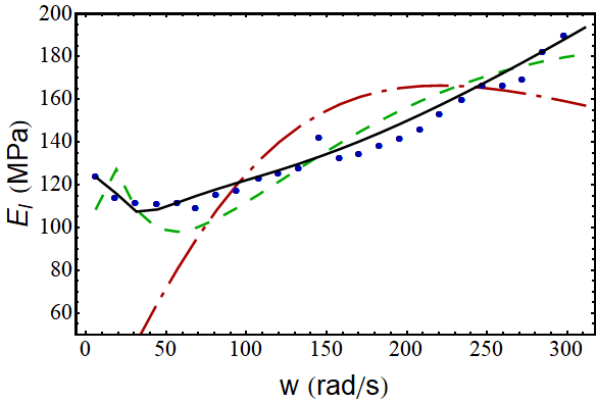

Fig. 4: Variation of storage (E_s) and loss moduli (E_l) with excitation frequency (w) for fiber angle (Ψ) = 45 degree. Key same as in Fig. 3.

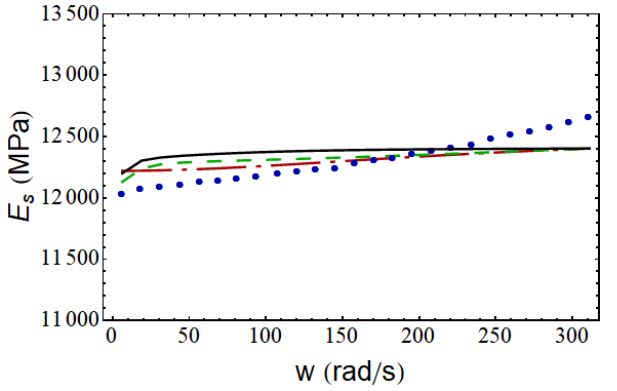

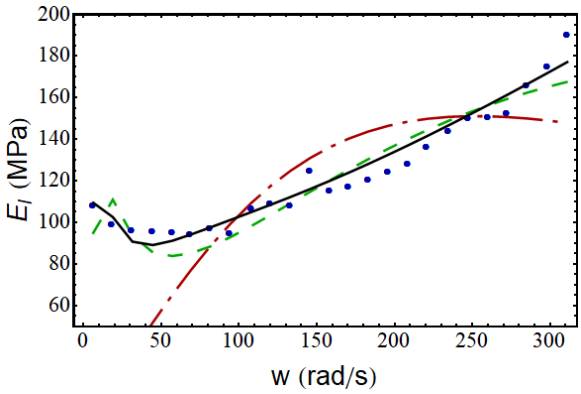

Fig. 5: Variation of storage (E_s) and loss moduli (E_l) with excitation frequency (w) for fiber angle (Ψ) = 90 degree. Key same as in Fig. 3.

Table 4: Maximum % error for various parametric model at different angles

Model	Modulus	0 Degree (%)	45 Degree (%)	90 Degree (%)
3 Parameter	E_s	1.69	1.58	1.99
	E_l	92.43	92	93.02
5 Parameter	E_s	1.38	1.53	2
	E_l	11	12	12
7 Parameter	E_s	2	2	2
	E_l	6	6	7

The model of E* obtained in the above analysis is in the direction 0, 45, 90 degree with the fiber. The method given in Jones [7] is used to obtain the value of E* at any angle Ψ with the principal axis.

$$\frac{1}{E_x^*} = \frac{1}{E_0^*}\cos(\Psi)^4 + \left[\frac{1}{G_{12}} - \frac{2\nu_{12}}{E_0^*}\right]\sin(\Psi)^2\cos(\Psi)^2 + \frac{1}{E_{90}^*}\sin(\Psi)^4 \quad (9)$$

Here, ν_{12}, G_{12} are the Poisson's ratio and shear moduli in the 1-2 plane respectively, E_0^*, E_{90}^*, E_{45}^* and E_x^* are the values of E* at 0 degree, 45 degree, 90 degree and at any arbitrary angle Ψ with 1 axis respectively and are represented as

$$E_0^* = E_{s0} + iE_{l0}\,,\ E_{90}^* = E_{s90} + iE_{l90} \text{ and } E_x^* = E_{sx} + iE_{lx} \quad (10)$$

$$\left[\frac{1}{G_{12}} - \frac{2\nu_{12}}{E_0^*}\right] = \left[\frac{4}{E_{45}^*} - \frac{1}{E_0^*} - \frac{1}{E_{90}^*}\right] \quad (11)$$

Fig. 6 shows the variation of storage and loss moduli with angle Ψ. In the figures as w increases (outwards from the origin), both the storage and loss modulus increases but the effect is more predominantly seen on the loss modulus.

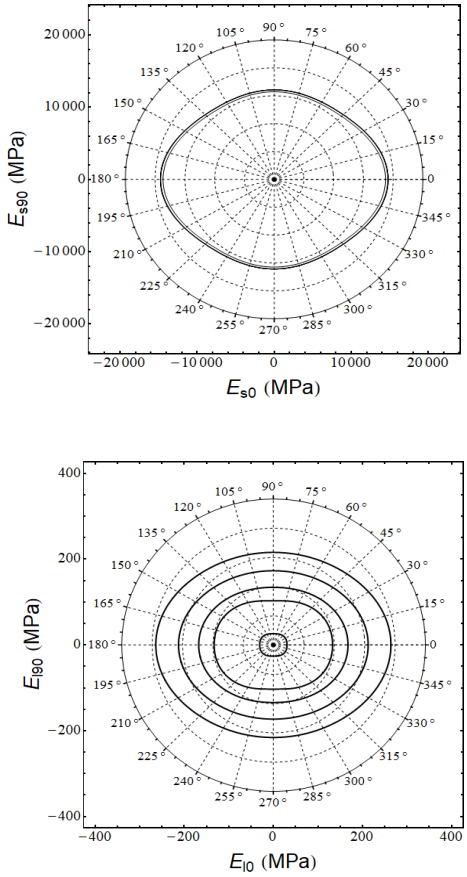

Fig. 6: Polar plot showing variation of Storage and Loss modulus with Ψ at different values of w (increases outwards from the origin)

Fig. 7a) shows the variation of loss modulus with increasing angular frequency. As the frequency of excitation increases the dampers present in the model (represented as combination of springs and dampers) began to freeze and thus loss modulus begins to drop after a particular frequency, the process continues till all the dampers get jammed, at this point loss modulus approaches zero and the resultant magnitude of the modulus approaches a constant value Fig. 7b), i.e. it fully becomes solid, thus, material should be used below this frequency otherwise damping will not come into action.

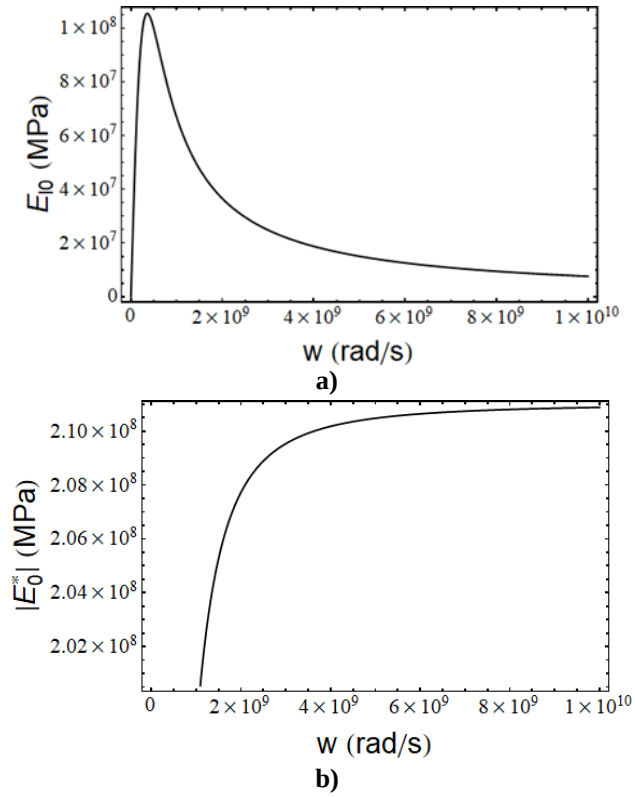

Fig. 7: Variation of a) loss modulus and b) total modulus with excitation frequency respectively

Thus parameters obtained by model extraction for 7 parameter model for coupling link with fiber angle at 0 degree. (Table 4 and following Eq. 16). The modulus of elasticity in operator from is:

$$E_0^*(\,) = 14422.44 + \frac{253.745D}{8.692+D} + \frac{104.447D}{86.291+D} + \frac{2.11\times10^8 D}{3.571\times10^8+D} \quad (12)$$

1.2. Calculation of coupling stiffness and damping

In a segmented disc coupling shown in Fig 8, two hubs are fitted, one each on the driver and driven shaft. The links (which are actually the segmented discs) are bolted alternatively on the hubs (i.e. one end of the link is bolted on driver hub and the other is bolted on the driven hub), so each hub has bolt holes half the no. of links used if ends of the consecutive links overlap. These links are also called disc packs, flex elements, flex blades or flex packs. These flex elements undergo deflections to accommodate misalignment. The links can also be connected in other ways, the idea of which can be get from [8- 10].

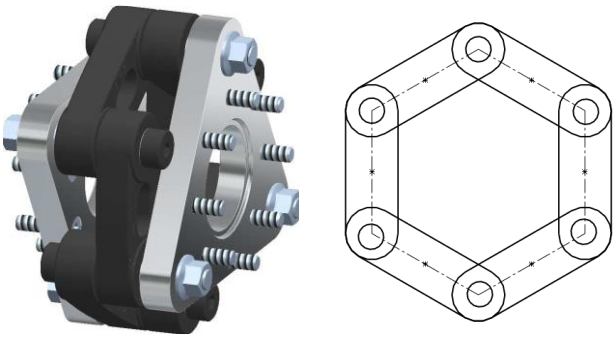

Fig.8: Ship Motion Group 6 link segmented disc coupling with side view of links

1.2.1 Parallel misalignment

The Fig. 9 shows the sketch of a general n-link coupling with alternate bolts attached to driver and driven ends of the hub, as explained above. In this, an even number of links are assumed to connect the two hubs. The ξ-η reference frame is assumed to be the spin-synchronized frame. Let $\triangle_\xi$ and $\triangle_\eta$ be small instantaneous displacements (of one hub of the coupling with respect to its other hub) along ξ and η directions respectively. Smallness of deflection is assumed to ensure linear behavior of the link material.

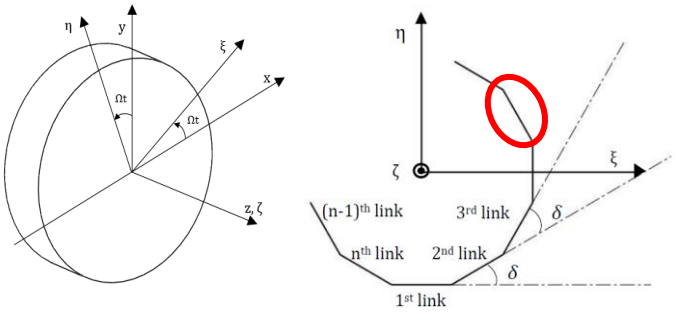

Fig. 9: Generalized n-link coupling orientation and angles

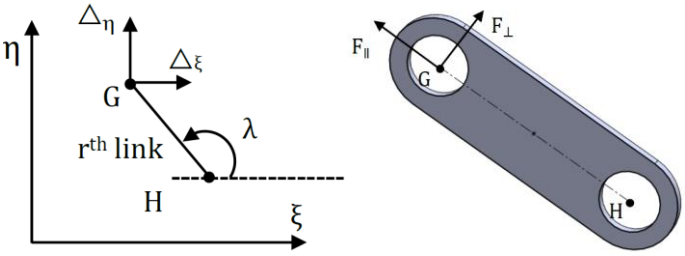

Fig. 10: Deflections in the r^{th} link

For any closed regular polygon of side n, the exterior angle between two consecutive links δ is equal to $\frac{2\pi}{n}$ radian. In Fig. 10 let λ be the angle made by the r^{th} link with ξ axis where, $\lambda = \delta(r-1)$. Let $\Delta_\parallel$ and $\Delta_\perp$ be the deflections of the head of the link (link end G) with respect to the base (link end H) parallel and perpendicular to the r^{th} link respectively which are given by

$$\begin{bmatrix} \Delta_\parallel \\ \Delta_\perp \end{bmatrix} = R * \begin{bmatrix} \Delta_\xi \\ \Delta_\eta \end{bmatrix} \quad (13)$$

Here, R is rotation matrix given by $\begin{bmatrix} \cos(\lambda) & -\sin(\lambda) \\ \sin(\lambda) & \cos(\lambda) \end{bmatrix}$

Each link described above acts like a beam element, the ends of which are rigidly fixed, to ensure that they are aligned perfectly with the hub at the point of fixation. This ensures that the end slopes are always zero despite the fact that they deflect

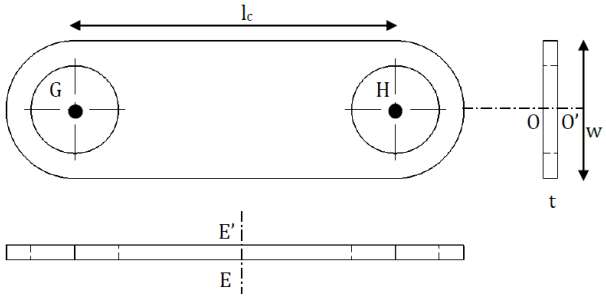

Fig. 11: Single link of coupling

Since the links are alternately bolted on the driver and the driven hubs, the net moment comes out to be zero, as shown in Fig. 12 below, for a 4-link coupling.

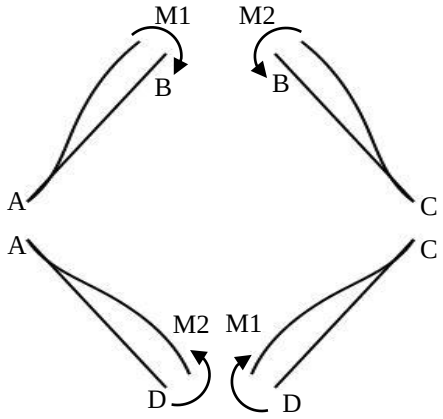

Fig. 12: Moments after deflection in a 4-link coupling

In general, the forces parallel and perpendicular to r^{th} link, $F_\parallel$ and $F_\perp$ respectively, are given by

$F_\parallel = k_1 \Delta_\parallel$ and $F_\perp = k_2 \Delta_\perp$ (14)

In the above, the expressions of stiffness k_1 and k_2 are given by $k_1 = AE_c/l$ and $k_2 = 12E_cI/l_c^3$, l_c is length of the link, E_c is modulus of elasticity of coupling material, A is area of cross section = w t, w is width and t is thickness, I is the area moment of inertia of the link (G-H) about neutral axis OO' of the link as shown in Fig 11. Therefore, the component of forces along ξ and η directions at any instant of time is given by

$$\begin{pmatrix} F_\xi \\ F_\eta \end{pmatrix} = R^T * \begin{pmatrix} F_\parallel \\ F_\perp \end{pmatrix} \quad (15)$$

R^T is the transpose of the rotation matrix R as given above.

Summing all such forces for all the links. The force acting on the hub F_{t1} and F_{t2} in the ξ and η directions respectively are obtained as

$$F_\xi^t = \sum_{r=1}^{n} F_\xi \text{ and } F_\eta^t = \sum_{r=1}^{n} F_\eta \quad (16)$$

$$F_\xi^t = k \triangle_\xi \text{ and } F_\eta^t = k \triangle_\eta \quad (17)$$

Here k denotes the equivalent lateral stiffness of the coupling. Variation of k with the no. of links is shown in Section 2.

If similar links are used as the sides of the regular polygon to connect the hubs, then coupling stiffness becomes same in both ξ & η directions. They will certainly be different if the links are dissimilar. Therefore, using similar links forming the sides of a regular polygon, produces isotropic stiffness of the coupling.

1.2.2 Angular misalignment

The orientation of n link coupling is shown again to define angular misalignment in the Fig. 13. Here 1, 2, 3…. n-1, n represents location of 1st, 2nd, 3rd ……. nth bolt respectively as seen in the end view; a similar view was given in Fig. 9.

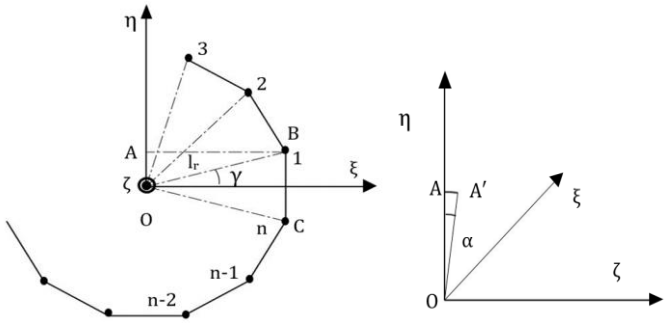

Fig. 13: Generalized n link coupling bolt orientation and angles

Here γ is the half interior angle given by, $\gamma = \frac{\pi}{n}$ radian. Let l_c be the length of a single link (BC) of the coupling, then $l_r = \frac{l_c}{2\sin(\gamma)}$

Let α, β be the angular deflections measured in the clockwise sense about ξ and η axes respectively. Fig.13 explains the angular deflection of the link by an angle α considered clockwise about the ξ axis. In this process OA moves to OA'.

The component of the OA in the ζ direction is found out as Δτ = AA' = OA *α, where chordal length between "A" and A' is considered almost same as the arc length, with an assumption that α is small angle lying between 1-4 degrees. Putting the value of OA, $\Delta\tau = l_r \sin(\gamma)\,\alpha$.

Therefore, the force in the direction of ζ for angular deflection α,

$$F_\zeta = k_3 \Delta\tau \quad (18)$$

where, k_3 is $12E_c I_1/l^3$, I_1 is area moment of inertia about neutral axis EE' (Fig. 11) of the link.

Moments due to this force about ξ and η axis are given as

$$M_{\xi\alpha} = F_\zeta OA = \alpha\, k_3\, l_r^2 \sin^2(\gamma) \quad (19)$$

$$M_{\eta\alpha} = -F_\zeta OB = -\alpha\, k_3\, l_r^2 \sin(\gamma)\cos(\gamma) = -\alpha\, k_3\, l_r^2 \sin(2\gamma)/2 \quad (20)$$

Since alternate bolts are present on the same hub, angle made with the ξ axis by different bolts are given by γ, 5γ, 9γ…. etc. This means that the r^{th} bolt will make an angle of (4r-3)γ with the ξ- axis. The total moment is the summation of the moment due to all links.

Summation of all the forces comes out to be zero as half of the coupling goes inside while other half comes out, if the number of links is chosen even.

$$\sum M_{\xi\alpha} = \alpha\, k_3\, l_r^2 (\sin^2(\gamma) + \sin^2(5\gamma) + \sin^2(9\gamma)\ldots) = \alpha\, k_b \quad (21)$$

$$\sum M_{\eta\alpha} = -\alpha\, k_3\, l_r^2 (\sin(2\gamma) + \sin(2(5\gamma)) + \sin(2(9\gamma))\ldots)/2 = -\alpha k_{bc} \quad (22)$$

Similarly moments due to angular deflection β about η axis is given by

$$M_{\xi\beta} = -\beta\, k_3\, l_r^2 \sin(2\gamma)/2 \text{ and } M_{\eta\beta} = \beta\, k_3\, l_r^2 \cos^2(\gamma) \quad (23)$$

$$\sum M_{\xi\beta} = -\beta\, k_3\, l_r^2 (\sin(2\gamma) + \sin(2(5\gamma)) + \sin(2(9\gamma))\ldots)/2 = -\beta k_{bc} \quad (24)$$

$$\sum M_{\eta\beta} = \beta\, k_3\, l_r^2 (\cos^2(\gamma) + \cos^2(5\gamma) + \cos^2(9\gamma)\ldots) = \beta\, k_b \quad (25)$$

Here, k_b and k_{bc} denotes the equivalent bending stiffness and cross couple bending stiffness of the coupling respectively. Values of k_b and k_{bc} for different no. of links is given in the Section 2.

From here we get equivalent total moments due to α and β as

$$M_\xi^t = \alpha\, k_t - \beta\, k_{bc} \text{ and } M_\eta^t = \beta\, k_t - \alpha\, k_{bc} \quad (26)$$

For number of links greater than six k_{bc} is zero (Appendix 1), thus

$$M_\xi^t = \alpha\, k_b \text{ and } M_\eta^t = \beta\, k_b \quad (27)$$

Since even number of links, or in that sense, the number of bolts is even, so due to any angular movement between the two hubs, about their diameter, half of the bolts will deflect in one direction and the other half will go to the opposite direction from a hypothetical mean nominal plane when the hubs are parallel. Under this situation, use of similar links arranged as sides of a regular polygon are shown in Fig 9. Equal and opposite forces will result for the pair of diametrically opposite bolts causing no net force. However, there will be a net moment. This also means, that if the links are dissimilar, or no. of links are not even, such a conclusion will not be true. Possibly for this reason, any coupling with odd no. of links is never used.

2. Results and Discussions

The equivalent material model and the stiffness values will now be combined to obtain an operator based stiffness.

Table 5: Variation of stiffness k with no. of links n as calculated in parallel misalignment

No. of links	Stiffness (k)
4	$2(k_1 + k_2)$
6	$3(k_1 + k_2)$
8	$4(k_1 + k_2)$
n	$0.5\,n\,(k_1 + k_2)$

Here $k_1 = AE_c/l_c$ and $k_2 = 12E_cI/l_c^3$ (28)

Table 6: Variation of stiffness k_b and k_{bc} with no. of links n as calculated in angular misalignment

No. of links	k_b	k_{bc}
4	$k_3 l_r^2$	$k_3 l_r^2$
6	$1.5\ k_3 l_r^2$	0
8	$2\ k_3 l_r^2$	0
10	$2.5\ k_3 l_r^2$	0
n	$0.25\ n\ k_3 l_r^2$ (n > 4)	0

Here k_3 is $12E_c I_1/ l_c^3$, I_1 is area moment of inertia about neutral axis EE' (Fig. 10) of the link.Ω
Thus equivalent coupling stiffness operator for no. of links greater than 6 is given as

$$\begin{bmatrix} k & 0 & 0 & 0 \\ 0 & k & 0 & 0 \\ 0 & 0 & k_b & 0 \\ 0 & 0 & 0 & k_b \end{bmatrix}$$

Operator based Stiffness

To obtain the operator based stiffness, the modulus of elasticity $E_0^*(\ )$, obtained in Eq. 12 is put in place of E_c in Eq. 28, then

$k(\ ) = 0.5\ n\ (A/ l_c + 12I/l_c^3)\ E_0^*(\ )$ and (29)

$k_b(\ ) = 3\ n\ (l_r^2\ I_1/ l_c^3)\ E_0^*(\ )$ (30)

The operator obtained above is operated as given below.
Let $\delta = \delta_0 e^{i\Omega t}$ be any sinusoidal deflection for such a coupling material, then the force due to such deflection is given as

$F = F_0^* e^{i\Omega t}$ where F_0^* is complex, also (31)

$F = k(\ )\ \delta$ (32)

$$F_0^* e^{iwt} = 0.5n(A/ l_c + 12I/l_c^3)((14422.44 + \frac{253.745D}{8.692+D} + \frac{104.447D}{86.291+D} + \frac{2.11\times10^8 D}{3.571\times10^8+D})\ \delta_0 e^{i\Omega t}) \quad (33)$$

The net numerator and denominator are operated on both sides to obtain the value of k* as F_0^*/δ in terms of frequency Ω as

$$k^* = 0.5\ n\ (A/ l_c + 12I/l_c^3)\ (\frac{(2.11\times10^8)((1.83\times10^7 i)-(2357658.876)\Omega-(25108.68i)\Omega^2+\Omega^3)}{((-8.692i)+\Omega)((-86.29i)+\Omega)((-3.576\times10^8 i)+\Omega)}) \quad (34)$$

Similarly $k_b^* = (3\ n\ l_r^2\ I_1/ l_c^3)$

$$(\frac{(2.11\times10^8)((1.83\times10^7 i)-(2357658.876)\Omega-(25108.68i)\Omega^2+\Omega^3)}{((-8.692i)+\Omega)((-86.29i)+\Omega)((-3.576\times10^8 i)+\Omega)}) \quad (35)$$

The values of these stiffness depend on material model, dimension and number of links (n) of the coupling. The width (w) and thickness (t) of the link are divided by its length 'l_c' to get non-dimensional parameters $w_0 = w/l_c$, $t_o = t/l_c$. For the stiffness two non-dimensional parameters k_0 (lateral stiffness ratio) = k^*/ K_s and k_{b0} (bending stiffness ratio) = k_b^*/K_s are used, where $K_s = k_1$ (when Ω = 0), is static stiffness of single link.
Thus,

$$k_0 = (\frac{6.934\times10^{-10} n(7.21\times10^8 t_0 w_0 + 7.211\times10^8 t_0 w_0^3)}{t_0 w_0})\ (\frac{(2.11\times10^8)((1.83\times10^7 i)-(2357658.876)\Omega-(25108.68i)\Omega^2+\Omega^3)}{((-8.692i)+\Omega)((-86.29i)+\Omega)((-3.576\times10^8 i)+\Omega)}) \quad (36)$$

Thus k_0 may be written as $k_0 = k_{0s} + i\ k_{0l}$, where k_{0s} and k_{0l} represent in-phase stiffness and the in-quadrature parts respectively.
Similarly

$$k_{b0} = 0.003125 n t_0^2 \operatorname{cosec}(\frac{\pi}{n})^2\ (\frac{(2.11\times10^8)((1.83\times10^7 i)-(2357658.876)\Omega-(25108.68i)\Omega^2+\Omega^3)}{((-8.692i)+\Omega)((-86.29i)+\Omega)((-3.576\times10^8 i)+\Omega)}) \quad (37)$$

$k_{b0} = k_{b0s} + i\ k_{b0}$ (38)

Table 7: Details of links in the coupling (Refer to Fig.11)

Length of link (l_c)	50 mm
Thickness of link (t)	1 mm
Width of link (w)	26 mm

Fig. 14 a) and b) show the variations of in-phase and in-quadrature parts of the lateral stiffness ratio of the coupling respectively. The value of k( ) derived in the Eq. 29 depends upon the dimension of the link, number of links and elastic modulus of the coupling (E_c). The value of E_c as obtained in the section 1.1 is represented by the 7 parameter model, is frequency dependent and contains both storage and loss parts. Similarly k_0 (lateral stiffness ratio) is proportional to E_c multiplied by a factor dependent upon link dimension and number of links. Thus the Figures 14a) and 14b) follow the same trend as followed by E_c (Fig. 3, 7 parameter model). Storage modulus increases with Ω but the effect of Ω on loss part is more dominant than on the storage and the loss part follows the material behavior of the coupling link as obtained from DMA. It is also seen that as the number of links of the coupling increases the coupling stiffness increases which can also be seen from the below figures.

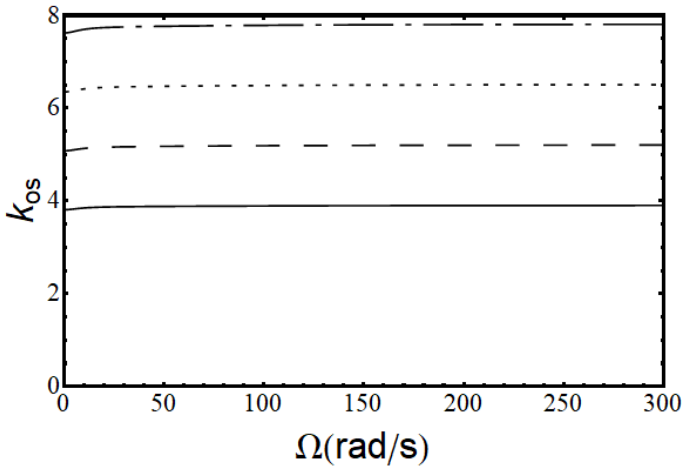

a)

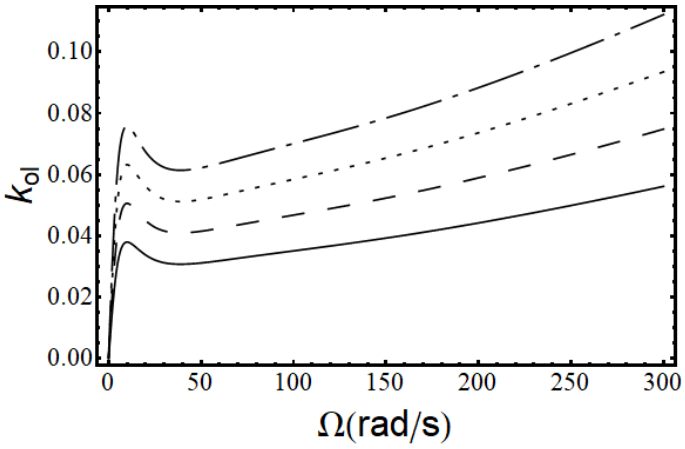

b)

Fig. 14a) and b): Variation of in-phase and in-quadrature value of lateral stiffness coefficient (k_0) with excitation frequency Ω for different no. of links. Key to the figure: no. of links (n) are represented as —— n = 6; – – – – n = 8; ..... n = 10; – · – · – n = 12;

3. Conclusions

- This work provides theoretical model to find the characteristics of segmented disc coupling with the help of viscoelastic model of the segment and net coupling stiffness and damping are obtained in terms of non-dimensional parameter for the coupling, making it useful irrespective of the shape and size of the coupling.
- The stiffness and damping of the coupling rotate with the spin synchronized rotor frame and thus it modifies the equivalent stiffness operator matrix of the system. Therefore, the coupling influences modal characteristics and response of the rotor shaft system. Most importantly the damping present in the coupling also acts as an internal damping and may cause instability.
- The coupling stiffness matrix obtained in this work can further be used to represent the coupling in the finite element modelling of coupled rotor-shaft system.
- The stiffness matrix in this work is obtained when misalignments from nominal position and given one at a time. The off-diagonal terms will also appear if the displacements are given simultaneously.

Acknowledgement

The authors like to gratefully acknowledge the kind help given by Mr. Anuj Bansal from North Street Cooling Towers Limited for supplying us with viscoelastic coupling links and the physical coupling for testing. The authors also acknowledge the help of Department of Science and Technology (DST), Government of India to grant a project titled “Design and fabrication of helicopter tail rotor shaft system using carbon-fiber reinforced composite” in this line through ECR/2018/001577 for continuing research activity in this direction.

References

1) Gibbons C.B., (1976), Coupling misalignment forces, Proceedings of the Fifth Turbo machinery Symposium, Gas Turbine Laboratory, Texas A&M University, TX, pp.111–11306.
2) Sekhar A.S., Prabhu B.S., (1995), Effects of coupling misalignment on vibration of rotating machines, Journal of Sound and Vibration 185, pp. 655–671.
3) Xu M., Marangoni R., (1994), Vibration analysis of a motor-flexible coupling-rotor system subjected to misalignment and unbalance—part I: theoretical model and analysis, Journal of Sound and Vibration 176, pp. 663–679.
4) Patel Tejas H., Darpe Ashish K., (2009), Vibration response of misaligned rotors, Journal of Sound and Vibration 325, 609–628.
5) Dutt J.K, Roy H, (2011), Viscoelastic modelling of rotor–shaft systems using an operator-based approach, Proc. IMechE Vol. 225 Part C: J. Mechanical Engineering Science, pp. 73-87.
6) Brinson and Brinson, (2015) Polymer Engineering Science and Viscoelasticity, Springer, 2nd Ed.
7) Robert Jones, (1998), Mechanics of Composite Materials, Second Edition, Taylor & Francis, pp. 74-81.
8) SGF,https://www.sgf.de/tl_files/theme/pdf_download/SGF%20CATALOG%20TENBEX-ECO%20SERIES.pdf
9) Ship motions products, http://shipmotiongroup.com/products.product+Flexible-coupling.page+1
10) Mancuso Jon R., (1999), Couplings and Joints, Design, Selection and Application, Second Edition, Marcel Dekker Inc.